Applications of Fe_3O_4@AC nanoparticles for dye removal from simulated wastewater

Seema Joshi[a], V. K. Garg[a,b*], Navish Kataria[b], K. Kadirvelu[c]

[a]*Department of Environmental Science and Engineering, Guru Jambheshwar University of Science and Technology Hisar-125001, India*

[b]*Department of Environmental Sciences and Technology, Central University of Punjab, Bathinda 151001, Punjab, India.*

[c]*Centre for Life Sciences, Bhartiyar University, Coimbatore – 641046,Tamilnadu, India*

Corresponding author: Phone +91-9812058109; email vinodkgarg@yahoo.com

Highlights:

- Fe_3O_4@AC nanoparticles were synthesised by co-precipitation methods for basic dye adsorption.
- Maximum adsorption capacity of Fe_3O_4@AC was 138 mg/g for MB and 166.6 mg/g for BG dye.
- Adsorption isotherms and kinetic and thermodynamic studies were also performed.
- Reusable potential of adsorbent was also evaluated upto several cycles.

Abstract:

This study deals with removal of cationic dyes from simulated wastewater using Fe_3O_4 nanoparticles loaded activated carbon. (Fe_3O_4@AC) nanoparticles were synthesised using co-precipitation methods. The Fe_3O_4@AC nanoparticles (nps) were characterised using different techniques and TEM anaysis revealed that the synthesized nanoparticles were 6 to16 nm in diameter. A pHpzc of Fe_3O_4@AC nanoparticles was 7.8. BET surface area of Fe_3O_4@AC nps was found 129.6 m^2/g by single point method and 1061.9 m^2/g by multipoint method. Adsorption experiments were performed to optimize the process conditions such as pH, nanoparticles dose, temperature, and concentration of dye and contact time. The maximum uptake capacity of Fe_3O_4@AC was 138 and 166.6 mg/g for methylene blue and brilliant green dyes, respectively. In order to assess dye adsorption behaviour, adsorption isotherm models viz., Langmuir, Freundlich and Temkin were applied. Langmuir isotherm best fitted [R^2= 0.993 (MB) and R^2=0.920 (BG)] to the experimental data of both the dyes. Further, Pseudo-second order rate equation fitted better to the experimental data. Reuse potential was

also investigated for both dyes and it is inferred from the data that the synthesised nanoadsorbent has promising reuse potential that can be used for several cycles.

Keywords: Methylene Blue; Brilliant green; Co-precipitation; Isotherms; Kinetics.

Introduction

Cationic dyes are extensively used in several industries such as packaging, textiles, paper and pulp, printing, leather, pharmaceutical etc. These dyes contain aromatic structure and azo groups (Yazdanbakhsh et al., 2011). Basic dyes [Brilliant green (BG) and Methylene blue (MB)] are often used by industries for colouring their products. These industries release dyes containing effluent into the wastewater streams that may cause several health problems including irritation in skin, eyes and gastro intestinal tract, vomiting, diarrhoea, coughing, vomiting etc (Saini et al., 2018; Zolgharnein et al., 2015). These dyes are toxic in nature and have non-biodegradable organic and inorganic compounds. These dyes also deteriorate the aquatic environment,. interrupt photosynthesis, growth of the aquatic life etc. Dye containing wastewater is hazardous and unfit to human life when discharged without any treatment (Joshi, S et al. 2018). Therefore, the treatment of dye laden industrial wastewater is unavoidable.

Different techniques such as ozonation, adsorption, advance oxidation process etc. have been adopted for wastewater treatments. Amongst these, adsorption is found to be more efficient, promising and having easy approach for treatment of dye amalgamated industrial wastewater (Kataria at al., 2016; Saini et al., 2017).]. However, choice of suitable adsorbent is hindered by several factors like cost; reuse potential, eco-friendly nature and field applications (Saini et al., 2017). Hence, it is important to develop and effective adsorbents. In recent times nanoadsorbents have emerged as a promising alternate. Nanoadsorbents can be employed for wastewater treatment due to their peculiar properties such as higher surface area, lesser production cost, higher efficiency, magnetic character etc. (Joshi et al., 2018; Kataria at al., 2016; Saini et al., 2017).

Recently, magnetite nanoadsorbents like Fe_3O_4@Ag/SiO_2 [2], Fe_3O_4@Sawdust carbon and EDTA@Fe_3O_4@Sawdust carbon (Kataria and Garg, 2018), sodium dodecyl sulphate modified $ZnFe_2O_4$ (Mahmoodi, 2015) and Fe_3O_4 loaded activated maize cob (Tan et al., 2012) are reported to have been prepared by surface modification. It is evident from these studies that surface modifications enhanced the physical as well as chemical properties of

nanoadsorbents, so that they become more usable for remediation of pollutants from industrial wastewater (Joshi et al., 2018; Kataria and Garg, 2018).

Activated carbon is extensively used for waste water treatment. But its application is restricted due to cost. Filtration used in this process also make water turbid and removal of turbidity is also a matter of concern (Mahmoodi, et al., 2011). But on combining this traditional adsorbent with nanonoadsorbent may make the process easier and cost effective because nanosize particles are cost effective and have reusable efficiency (Haldorai and Shim, 2014). The purpose of choosing and synthesizing Fe_3O_4@AC nps is based on following hypothesis: a) Activated charcoal contains negative sites (O^{2-} and OH^-) and Fe_3O_4 nanosphere also having enough O^{2-} (negative) sites around Fe^{2+} and Fe^{3+} which interacts with the positive sites of cationic dyes. It can enhance the removal percentage and adsorption capacity for cationic dye. b) Prepared Fe_3O_4@AC nps adsorbent exhibits magnetic property so it can be easily separated from waste water and c) Reusability of nanoadsorbents is found better than other traditional adsorbents. In the present work, iron oxide nanoparticles loaded activated charcoal was prepared to apply for dye removal from aqueous medium. It was prepared by co-precipitation method. Cationic dye adsorption was investigated by experiments performed in batch mode. Adsorption behaviour and rate mechanism were investigated by isotherm and kinetics modelling. Further, reuse potential of Fe_3O_4@AC nps for cationic dyes were checked for several cycles.

2. Experimentation

2.1. Reagents & Materials

Ferric nitrate hexahydrate, Tartaric acid, Sodium hydroxide pellets, Methylene blue dye (MB),Brilliant green (BG) dye and Activated Charcoal (phosphorous free) AR were purchased from SD fine-chemical Limited, Mumbai. AR grade of chemicals were used in the present study. More details of cationic dyes are given in Table S1.

2.2. Preparation of Fe_3O_4@AC nanoparticles:

Modified co-precipitation process was adopted to prepare Fe_3O_4@AC nps (Joshi et al., 2018; Tan et al., 2012). In first stage, solution of $FeCl_3$ (0.1M), $Fe(NO_3)_3.9H_2O$ (0.2M) and tartaric acid (0.05M) were prepared by mixing together in 100 mL double distilled water (DDW). The solution was stirred for 30 min. Thereafter, NaOH was added drop wise until brownish colour precipitates formed. Then, solution was stirred for 2hr and precipitate was filtered and

cleaned with DDW. Iron oxide nanoparticles so obtained, were put in oven at 80 °C for one hr. In second stage, one gram of synthesised nanoparticles was mixed in 70 mL of DDW and two grams of activated charcoal (AC) was added in this using ultra sonication method to avoid particle aggregation. The resultant blackish precipitate so obtained was dried in oven at 100°C for 120 min. to obtain the desired material. Scheme S1 shows the graphical representation of synthesis of Fe3O4@AC nps.

2.3. Characterization and Instrumentation

Particle Size:

Dynamic light scattering (DLS) method was used to find out the hydrodynamic diameter of prepared Fe_3O_4@AC nanoparticless by Zetasizer instrument.

XRD Analysis:

The crystalline structure of Fe_3O_4@AC nps was investigated by XRD technique via (Rigaku miniflex II Diffractometer), by Cu-K_α X-ray radiations at room temperature in the 2θ range of 20°-80°at scanning rate of 2˚/min.

TEM Analysis:

Transmission electron microscopy was performed to investigate the particle size of Fe_3O_4@AC nps by means of FEI Tecnai G^2 20 TWIN electron microscope at 200 KV.

FTIR Analysis:

To analyse the functional groups in the synthesised nanoadsorbents, FTIR study was performed using Shimadizu IR AFFINITY-1spectrophotometer using KBr powder pellet.

SEM Analysis:

The elemental analysis and morphology of surface of Fe_3O_4@AC nps were estimated via Scanning electron microscopic (SEM) technique and Energy-dispersive X-ray (EDX) analysis which was performed by Merlin compact 6073 scanning electron microscope (Carl Zeiss, Germany).

pH at point zero charge:

The pH at point zero charge was calculated by early reported $NaNO_3$addition method. Instrumentation details for characterisation are already reported in our previous studies. (Joshi et al., 2018; Saini et al., 2017).

2.4. Batch adsorption experiments

Batch mode study was undertaken under dark conditions, to optimize the different parameters (dye concentration, pH, adsorbent dose, time etc.). Dye adsorption experiments

were performed in 50mL of 50 mg/L of MB and BG dye solutions in an Erlenmeyer flask at room temperature (27±1˚C) using orbital shaker. Shaking speed used was 200 rpm. Adsorbent dosages were changed from 0.010 g to 0.040 g/50mL, dye concentration used was between 30 mg/L to 100 mg/L, mixing time was 20-120 min and solution pH was set from 2 to 10 by adding 0.01N solution of HCl or NaOH. The pH of solutions was measured by pH meter (Eutech Instruments, Singapore). UV-VIS spectrophotometer used to quantify the dye concentration. Centrifuge of Dye solutions containing Fe_3O_4@AC nps was performed at 10000 rpm for ten minutes. Absorbance was measured at λ_{max} 664 nm for MB dye and λ_{max} 626 nm for BG dye. Removal (%) of dyes and adsorption capacity for dyes were estimated using the following equations:

$$Dye\ removal\ (\%) = \frac{(C_o - C_e)}{C_o} \times 100 \quad (1)$$

$$Adsorption\ capacity\ (q_e) = \frac{(C_o - C_e)\,V}{m} \quad (2)$$

Where m in grams represents the mass of Fe_3O_4@AC nps, C_o in mg/L represent initial dye concentration, C_e in mg/L is equilibrium dye concentration, q_e in mg/g represent amount of dye adsorbed per unit of the adsorbent at equilibrium and volume of dye solution is V (L).

3. Results for discussion

3.1. Fe_3O_4@AC nps Characterization

Fig. 1a depicts the characteristic peaks of synthesized Fe_3O_4@AC nanoparticles in XRD patterns which were recorded using X-ray diffractrometer at 2θ= 30.3˚, 35.6˚, 45.5˚, 60˚and 65˚ and the observed peaks were matched to diffraction planes (511), (440), (422), (400) ,(311), and (220), respectively. These observations matched with earlier studies (Loh et al., 2008; Seyedsadjadi et al., 2014; Ding et al., 2012).

Fourier Transform Infra Red (FTIR) spectroscopy used in the present study was to find out the different functional groups and sites which are available for bindings of the synthesized nanoparticles. In Fig. 1b, the activated charcoal (AC) exhibits absorption bands at 3420 cm^{-1}, 3120 cm^{-1}, 2320 cm^{-1}, 1725 cm^{-1} and 1178 cm^{-1}. The broad peak at 3420 cm^{-1} is due to OH stretching of H-bond which shows the presence of hydroxyl group. The Fe_3O_4@AC exhibits absorption peaks at 2320 cm^{-1}, 3420 cm^{-1}, 1725 cm^{-1}, and 1588 cm^{-1}.

Here, two more peaks are observed at 698 cm^{-1} and 487 cm^{-1}which show the presence of iron oxide in the prepared sample (Reza and Ahmaruzzaman, 2015).

Scanning electron micrographs (Fig. 1c) were used to study surface morphologies and texture of Fe_3O_4@AC nps at different magnification. The SEM image reveals that the particles are not completely spherical. EDX image gives the elemental composition i.e. it contains iron, oxygen and traces of copper and chlorine as impurities as shown in Fig. 1d. DLS spectra were analysed using hydrodynamic size distribution of Fe_3O_4@AC nps. The size distribution of Fe_3O_4@AC nps was found in between 100-1000 d.nm as observed in Fig. 1e.

Nitrogen adsorption–desorption isotherm plots between relative pressure (P/P^o) and adsorbed volume (cc/g at STP) of Fe_3O_4@AC nps are shown in Fig. 1f. BET surface area of Fe_3O_4@AC nps at single point method and multipoint method was found to be 129.6 m^2/g and 1061.9 m^2/g, respectively. The values of BJH pore volume and pore diameter of adsorbent were 0.0206 cc/g and 3.6 nm, respectively. Total pore volume and Average pore diameter were found to be 0.54 cc/g, and 16.6 nm respectively.

TEM images are shown in Fig. 2a-d which reveal that nanoparticles are in the range of 6 -16 nm. Perusal of the Fig. 2 shows that the synthesized Fe_3O_4@AC nps are very fine and their cluster shows that activated charcoal is fully incorporated in Fe_3O_4 particles. SAED (selected area electron diffraction) pattern also indicates the low crystallianity of the synthesised Fe_3O_4@AC nps due to amalgamation of activated carbon as evidenced by broad diffraction rings in Fig. 2c. The pH at point of zero surface charge (pHpzc) of synthesized nanoparticles was 7.8, calculated from plot between ΔpH (pHi –pHf) versus pHi as given in Fig. 3a. At pH = 7.8, surface of material contains identical number of positive and negative charge functional groups or ions.

3.2. Batch Adsorption studies

3.2.1. The pH effect study

For both cationic dyes such as MB and BG, effect of pH was investigated within the pH range from 2 to10. The present study was performed with 0.025 g/50mL of dose in 50 mg/L of dye concentration at room temperature for 2 h. Perusal of the data presented in Fig. 3b shows that with increase in pH from 2 to 10, dye removal was also increased from 84.3 %to 100% and 55.6% to 91.8% for MB and BG dyes, respectively. The pH effect on dye exclusion can be understood by the competition between positive ions of cationic dyes and

H^+ ions at low pH. The pHpzc of Fe_3O_4@AC nanoparticle was 7.8 (Fig. 3b). The pH below pHpzc, surface of adsorbent was positively charged which repel cationic dye molecules. With increase in pH above pHpzc, negatively charged surface of adsorbent attract positively charged dye molecules and number of H^+ ions decreases rapidly causing less competition between H ions and cationic dye molecules adsorbed at active sites (Kataria and Garg, 2019). The result showed that the pH of the solution has significant effects on the adsorption, suggesting thereby that the ionization of the adsorbate and the surface charge are varied as the charge of pH of solution. The observed trend may also be explained as follows: At lower pH, the electrostatic repulsion between molecules of cationic dyes and H^+ ions of adsorbent surface is higher which results in less dye removal. At higher pH values, the surface adheres negative charge and thus the competition for H^+ ions becomes less which causes more dye removal (Wu et al., 2016; Ali et al., 2017; Saini et al., 2018).

3.2.2. Initial dye concentration and its effect

Fig. 3c depicts the effect of initial dye concentration (30 mg/L to 100 mg/L), on the removal of cationic dyes within the range of dye concentration, from the figure, showed the adsorption of dye molecules decreased with increase in dye concentration. At 30 mg/L, the removal was 100% for both MB dye and BG dye while at 100 mg/L the removal was only 69.9% for MB and 83.8% for BG. This might be due to accessibility of additional active sites on adsorbent surface for dye adsorption at low concentration of dyes while due to less availability of surface-active binding sites with increase in dye concentration because of saturation of binding site with dye molecule (Rehman et al., 2013; Wu et al., 2016; Saini et al., 2018) the dye removal tendency decreases.

3.2.3. Adsorbent dose effect

Effect of adsorbent dose for adsorption of cationic dyes was performed using 50 mL of dye solution with 50 mg/L of dye concentration at room temperature for two hours. The adsorption was changed in the range from 0.01 to 0.04 g (Fig. 3d). For BG dye, with increase in adsorbent dose, dye removal was continuously increased from 73.8 to 100 %. Similar behaviour was viewed in MB dye i.e., removal was increased from 94.3 to 100 %. Both the dyes achieved maximum adsorption at 0.04 g dose and which was 100 %. It may be due to accessibility of additional active binding sites and surface area for cationic dyes with increased in adsorbent dose (Wu et al., 2016; Jia et al., 2016; Kataria and Garg, 2017; Joshi et

al., 2018). However, when the dosage becomes 0.04g, the adsorbents afford adequate number of active sites that react completely with the molecules of cationic dyes.

3.2.4. Contact time and its effect

Fig. 3e, f shows the effect of contact time which varied from 0.0 to 120 min for both the MB and BG dyes. The batch mode studies were conducted in 250 mL Erlenmeyer flasks with 50 mL of dye solutions of different dye concentrations (30-100mg/L) using 0.025g/50 mL of adsorbent dose at 27±1˚C. There was fast enhancement in adsorption process with increase in contact time up to 20 min. It may be due to the availability of large number of free surface active sites for dye adsorption. Thereafter, was slight increase in dye removal and then attains equilibrium at 120 min. This suggests that no more active sites are produced for dye adsorption after the maximum surface area occupied by the dye molecule is attained (Duman et al., 2016; Kataria and Garg, 2019).

3.2.5. Effect of thermal treatment

The result of effect of temperature was obtained for MB and BG dyes, in range from 10 to 50˚C, with 50 mg/L dye concentration for 120 min. It was found that both the dyes showed almost identical behaviour with respect to variation of temperature as shown in Fig. 3g. The dye removal percentage was enhanced from 81% to 93.5 % for MB dye and 76.94% to 92.1% for BG dye, with increase in temperature. The phenomenon is attributed to the fact that the due to raise in temperature, the contact of dye molecules with the adsorbents surface active sites were also increases. Hence, it results in increased mobility and diffusion of cationic dye molecules in aqueous solution. The adsorption experiments were performed at room temperature (Bhagat et al., 2014; Kataria and Garg, 2017)**.**

3.3. Thermodynamic behaviour study

Parameters of thermodynamics such as changes in, (ΔS˚) entropy, (ΔG˚) Gibb's free energy and (ΔH˚) enthalpy for the adsorption of cationic dyes on Fe_3O_4@AC nps have been investigated by using temperature variation experiments. Following equations are made (Saini et al., 2018; Smith and Ness, 1987) use of:

$$\Delta G^0 = -RTlnK_d \quad (3)$$

$$K_d = \frac{C_a}{C_e} \quad (4)$$

$$lnK_d = -\frac{\Delta H^0}{RT} + \frac{\Delta S^0}{R} \quad (5)$$

Where K_d is the equilibrium constant, R is gas constant (8.314 J $mol^{-1}K^{-1}$), T (K) is temperature and C_a(mg/L) is the quantity of MB and BG dyes on the nanoadsorbent surface at equilibrium. The ΔH˚ and ΔS˚ were determined from the slope and intercept values of linear plots between lnK_d and 1/T (Fig. 3h). Table 1 illustrate that the adsorption process for both the dyes is endothermic due to positive values of ΔH˚, which in turn indicates that both the dyes are absorbed by physical process (Kataria and Garg, 2017). The positive value of ΔS˚ for MB dye (104.49 J $mol^{-1}K^{-1}$) and for BG dye (92.18 J $mol^{-1}K^{-1}$) confirm that the increase in the degree of mobility at the solid-solution interface which enhance the adsorption dye molecules. The adsorption feasibility and spontaneity for MB and BG dyes were ascertained by negative value of ΔG˚, which is illustrated in Table 1.

3.4. Adsorption Kinetics

Pseudo-first order (Langergren, 1898) and pseudo-second order (Mckay and Ho, 1999) models were made use of to investigate the rate mechanism of adsorption of cationic dyes onto prepared Fe_3O_4@AC nps. The linear forms are represented by the following expressions.

$$\log(q_e - q_t) = logq_e - \left(\frac{k_1}{2.303}\right)t \quad (6)$$

$$t/q_t = 1/k_2\, q_e^2 + t/q_e \quad (7)$$

$$q_t = k_{id}t^{1/2} + C \quad (8)$$

Where, (q_e) at equilibrium time is the adsorption capacity, (q_t) at time t is the adsorption capacity, k_1 (min^{-1}) is the rate constant for pseudo-first order, k_2 (min^{-1}) is the pseudo-second order rate constant. The parameters of kinetic models are illustrated in Table 2. It was calculated from the experimental data by applying linear regression analysis to the linear form of all the models. Fig. 4(a-d) depicts the linear plots of pseudo-first order and pseudo-second order models. The values of k_1, and q_e were found by the plot of log ($q_e - q_t$) vs t for pseudo-first order model and the plot of t/q_t versus t for the pseudo-second order model. The q_e (calculated) value determined from plot is less than q_e (experimental) value as illustrated in table for both the cationic dyes suggesting that the pseudo-first order was not best fitted while values of Pseudo-second order regression coefficient, (R^2 = 0.999) of both the basic dyes are

bigger than that of pseudo-first order which shows the applicability of the later, Also the q_e (cal) values are nearer to or almost equal to q_e (exp) values obtained from adsorption experiments of both the dyes for pseudo-second order model. Hence, pseudo-second order model is best suited for both the dyes.

For intraparticle diffusion model, k_{id} is intraparticle diffusion constant and C is intercept which gives the approximate boundary layer thickness. The values of k_{id} and C were getting from intercept and slope, respectively, of the curves of the plot between q_t versus $t^{1/2}$. Intraparticle model, assumed that both the dye molecules (BG and MB) were moving towards the pores of the adsorbents from bulk solutions through boundary layers (Kataria and Garg, 2018a). Table 3 shows the higher values of C for MB and BG dyes which suggest the involvement of boundary layer thickness for cationic dyes adsorption. Two different linear curves are shown in Fig 4(e,f) suggesting the involvement of two stage process for both the cationic dyes adsorption. Firstly, bulk of dye molecules migrated towards boundary layer of adsorbent. Secondly, linear layer shows the intraparticle diffusion and then achieving equilibrium hence, the rate mechanism of cationic dye adsorption was controlled by intraparticle diffusion and boundary layer diffusion both.

3.5. Equilibrium isotherm models

Adsorption behaviour and interaction between adsorbent and dye molecules were interpreted using isotherm models (Langmuir, 1916). Langmuir, Freundlich and Temkin & Pyzhev adsorption isotherm models were applied to the adsorption data to explain the adsorption equilibrium of cationic dyes onto Fe_3O_4@AC nps. Linear form of Langmuir isotherms model (Langmuir, 1918) is given as.

$$\frac{C_e}{q_e} = \frac{1}{q_{max}b} + \frac{C_e}{q_{max}} \quad (9)$$

Where *b* (L/mg) is the Langmuir constant, q_{max} (mg/g) is the maximum monolayer adsorption capacity.

Freundlich isotherms model (Freundlich, 1906) may be represented by the equation:

$$logq_e = logK_f + \frac{1}{n}logC_e \quad (10)$$

Where K_f is a Freundlich constant (related to adsorption capacity) and 1/*n* is the heterogeneity factor (related to intensity of adsorption) and its value should be lie within 0 and 1 to make adsorption process favourable. The value of 1/n near zero indicates heterogeneous surface,

1/n less than 1, indicates chemisorption and 1/n greater than 1, indicates cooperative adsorption (Foo and Hameed, 2010, Kataria and Garg, 2019)

Temkin isotherms model (Temkin and Pyzhe, 1940) is given by the expression:

$$q_e = BlnK_T + BlnC_e \quad (11)$$

Where R (8.314 J $mol^{-1}K^{-1}$) is the gas constant, $B = RT/b$, b (J/mol) is the Temkin constant which indicates the heat of adsorption, T (K) is absolute temperature and K_T (L/g) is equilibrium binding constant. Correlation coefficients and Model parameters for MB dye and BG dye are encapsulated in Table 3. The linear plots of isotherm models are shown in Fig. 5(a-c). The highest correlation coefficient for MB dye (R^2 = 0.993) and BG dye (R^2 = 0.920) were found using Langmuir model. comparison of studied isotherms models suggested that the Langmuir model better described the adsorption of both the dyes than Temkin and Freundlich model. This shows the monolayer adsorption of cationic dyes on Fe_3O_4@AC nps. The maximum adsorption capacity of MB and BG dyes were 138.8 mg/g and166.6 mg/g, respectively. The adsorption capacities of MB and BG dyes with other reported adsorbents are listed in Table 4. This information suggest that the Fe_3O_4@AC nps have potential to remove cationic dyes from simulated waste water.

3.6. Adsorption mechanism for dye removal onto Fe_3O_4@AC nps

Adsorption by nanoparticles for cationic dye elimination is influence by several factors such as availability of functional groups, surface charge, pH etc .These factors determines the mechanism of the investigation related to dye adsorption behaviour (Kataria and Garg, 2019). In the present work, iron oxide nanoparticles loaded activated charcoal was prepared to apply for dye removal from aqueous medium. Here the possible mechanism was explained on the basis of surface charge and functional groups present on both the adsorbate and adsorbent system. Activated charcoal contains negative sites (O^{2-} and OH^-) which interact with positive ions. Similarly, Fe_3O_4 nanosphere also having lots of available O^{2-} (negative) sites around Fe^{2+} and Fe^{3+} atom which interacts with the positive sites of both the cationic BG and MB dye. Furthermore when we utilize iron oxide nanoparticles loaded activated charcoal Fe_3O_4@AC then we got more negative active available sites for our experimental system of basic dyes removal which enhances the interaction among adsorbent and adsorbate surface hence, there is increase in removal percentage and adsorption capacity for cationic dye removal by synthesised nanoadsorbent. (Saini et al., 2018). Fig.6 shows the possible adsorption mechanism for dye removal onto Fe_3O_4@AC nps.

3.7. Reuse Potential of Adsorbent

In the present work, reusability of the Fe_3O_4@AC nps was investigated by performing four cycles of dye removal experiments as shown in Fig.5d. The adsorbent was separated from the aqueous medium by centrifugation, after the completion of adsorption experiments. Thereafter it was washed using ethanol and distilled water for a number of times then dehydrated in oven for few hours at 80 °C. The regenerated adsorbent was further used for adsorption of cationic dyes. In the first cycle the removal percentages for BG dye was 74.5% and for MB dye 79.2% respectively. After third cycle, the removal (%) was slightly reduced in for both the dyes and thereafter, became constant in fourth cycle as shown in Fig. 5d. It suggests that Fe_3O_4@AC nps have good reusable efficiency and can be used for several cycles.

4. Conclusions.

In this work Fe_3O_4@AC nps have been synthesised by co-precipitation method and exhibited good adsorption behaviour towards cationic dyes under the optimum process conditions. Further its efficiency was compared with other synthesised nanoadsorbents for cationic dyes removal and it was found to be more efficient than others. The maximum adsorption capacities for MB and BG dyes were found to be138 mg/g and 166.6 mg/g, respectively. Langmuir model is best fitted in dye adsorption data which indicates the monolayer adsorption of dye molecules on the surface of Fe_3O_4@AC nps. Pseudo-second order model was suited in both the cationic dyes adsorption data. This observation reveals that the Fe_3O_4@AC nanoadsorbent has a significant potential for the adsorption of MB and BG dyes from aqueous medium and can be reused for several cycles successfully.

Acknowledgement

One among the authors (Ms. Seema Joshi) is thankful to University Grants Commission, New Delhi India for providing the financial assistance inthe form of BSR-UGC Fellowship.

References

Ahmad, R., Kumar, R., 2010. Kinetic and thermodynamic studies of brilliant green adsorption onto carbon/iron oxide nanocomposite. J. Korean Chem. Soc. 54, 125-130.

Ahmed, M.J.K., Ahmaruzzaman, M. (2015). A facile synthesis of Fe3O4–charcoal composite for the sorption of a hazardous dye from aquatic environment. J. Environ. Manage. 163, 163-173.

Ali, A.F., Kovo, A.S., Adetunji, S.A., 2017. Methylene Blue and Brilliant Green Dyes Removal from Aqueous Solution Using Agricultural Wastes Activated Carbon. Journal of Encapsulation and Adsorption Sciences. 7, 95-107.

Arivoli, S., Hema, M., Parthasarathy, S., Manju, N., 2010. Adsorption dynamics of methylene blue by acid activated carbon. J. Chem. Pharm. Res, 2(5), 626-641.

Asadullah, M., Asaduzzaman, M., Kabir, M.S., Mostofa, M.G., Miyazawa, T., 2010. Chemical and structural evaluation of activated carbon prepared from jute sticks for Brilliant Green dye removal from aqueous solution. J. Hazard. Matter. 174, 437-443.

Bahgat, M., Farghali, A.A., El Rouby, W.M.A., Khedr, M.H., 2014. Efficiency, Kinetics and Thermodynamics of Toluidine Blue dye removal from aqueous solution using MWCNTs decorated with $NiFe_2O_4$. Fuller Nanotub. Car N. Structures 22, 454-470.

Chen, J., Feng, J., Yan, W., 2016. Influence of metal oxides on the adsorption characteristics of PPy/metal oxides for Methylene Blue. J. Colloid Interfac Sci. 475, 26–35.

Ding, H.L., Zhang, Y.X., Wang, S., Xu, J.M., Xu, S.C., Li, G.H., 2012. Fe_3O_4@SiO_2 Core/Shell nanoparticles: the silica coating regulations with a single core for different core sizes and shell. Chem. Mater. 24, 4572–4580.

Duman, O., Tunç, S., Polat, T.G., Bozoğlan, B.K., 2016. Synthesis of magnetic oxidized multiwalled carbon nanotube-κ-carrageenan-Fe_3O_4 nanocomposite adsorbent and its application in cationic Methylene Blue dye adsorption, Carbohydr. Polym.147, 79-88.

Freundlich, H. M. F., 1906. Over the Adsorption in Solutions. J. Phys. Chem. 57, 385-471.

Ghaedi, M., Heidarpour, S., Kokhdan, S.N., Sahraie, R., Daneshfar, A., Brazesh, B., 2012. Comparison of silver and palladium nanoparticles loaded on activated carbon for efficient removal of methylene blue: kinetic and isotherm study of removal process. Powder Technol. 228, 18-25.

Ghaedi, M., Hossainian, H., Montazerozohori, M., Shokrollahi, A., Shojaipour, F., Soylak, M., Purkait, M.K., 2011. A novel acorn based adsorbent for the removal of brilliant green. Desalination, 281, 226-233.

Ghaedi, M., Negintaji, G., Marahel, F., 2014. Solid phase extraction and removal of brilliant green dye on zinc oxide nanoparticles loaded on activated carbon: new kinetic model and thermodynamic evaluation. J. Ind. Eng. Chem. 20, 1444-1452.

Haldorai, Y., Shim, J., 2014. An efficient removal of methyl orange dye from aqueous solution byadsorption onto chitosan/MgO composite: A novel reusable adsorbent. Appl. Surf. Sci. 292, 447– 453.

Jia, Z., Li, Z., Li, S., Li, Y., Zhu, R., 2016. Adsorption performance and mechanism of methylene blue on chemically activated carbon spheres derived from hydrothermally-prepared poly (vinyl alcohol) microspheres. J. Mol. Liq. 220, 56-62.

Joshi, S., Garg, V.K., Saini, J., Kadirvelu, K., 2018. Removal of Toulidine Blue O Dye from Aqueous Solution by Silica-Iron Oxide Nanoparticles. Mater. Focus. 7, 146–147.

Kataria N., Garg, V.K., 2018a. Optimization of Pb (II) and Cd (II) adsorption onto ZnO nanoflowers using Central Composites Design: Isotherms and Kinetics Modelling. J. Mol Liq. 271, 228-239.

Kataria, N., Garg, V.K., 2017. Removal of Congo red and brilliant green dyes from aqueous solution using flower shaped ZnO nanoparticles. J. Environ. Chem.Eng. 5, 5420-5428.

Kataria, N., Garg, V.K., 2018b. Green synthesis of Fe_3O_4 nanoparticles loaded sawdust carbon for Cadmium (II) removal from water: regeneration and mechanism. Chemosphere. 208, 818–828.

Kataria, N., Garg, V.K., 2019. Application of EDTA modified Fe_3O_4/sawdust carbon nanocomposites to ameliorate methylene blue and brilliant green dye laden water. Environ. Res. 172, 43–54.

Kataria, N., Garg, V.K., Jain, M., Kadirvelu, K., 2016. Preparation, characterization and potential use of flower shaped Zinc oxide nanoparticles (ZON) for the adsorption of Victoria Blue B dye from aqueous solution. Adv. Powder Technol. 27, 1180–1188.

Langergren, S., Svenska, B. K., 1898. Zur Theorie der Sogenanaken Adsorption. Geloster Stoffe Veterns Apsakad Handle 24, 1-39.

Langmuir, I., 1916. The constitution and fundamental properties of solids and liquid. J. Am. Chem. Soc. 38, 2221–2295.

Langmuir, I., 1918. The adsorption of gases on plane surface of glass, mica and platinum. J. Amer. Chem. Soc. 40, 136-1403.

Loh, K.S., Lee, Y. H., Musa, A., Salmah, A. A., Zamri, I., 2008. Use of Fe_3O_4 nanoparticles for enhancement of biosensor response to the herbicide 2, 4-dichlorophenoxyacetic acid. Sensors. 8, 5775–5791.

Mahmoodi, N. M., 2015. Surface modification of magnetic nanoparticle and dye removal from ternary systems. J. Ind. Eng. Chem. 27, 251–259.

Mahmoodi, N.M., Salehi, R., Arami, M., 2011. Binary system dye removal from colored textile wastewater using activated carbon: Kinetic and isotherm studies. Desalination, 272, 187-195.

Mane, V.S., Mall, I.D., Srivastava, V.C., 2007. Kinetic and equilibrium isotherm studies for the adsorptive removal of Brilliant Green dye from aqueous solution by rice husk ash. J. Environ. Manage. 84, 390-400.

Mckay, G., Ho, Y. S., 1999. Pseudo-second order Model for Sorption Processes. Process. Biochem. 34, 451-465.

Mu, B., Tang, J., Zhang, L., Wang, A., 2016. Preparation, characterization and application on dye adsorption of a well-defined two-dimensional superparamagnetic clay/polyaniline/Fe_3O_4 nanocomposite. Appl. Clay Sci. 132, 7-16.

Mubarak, N. M., Fo, Y. T., Hikmat Said Al-Salim., Sahu, J. N., Abdullah, E. C., Nizamuddin, S., Jayakumar N. S. And Ganesan, P. 2015. Removal of Methylene Blue and Orange-G from WasteWater Using Magnetic Biochar. Int. J. Nanosci. 14, 1-13.

Nourmoradi, H., Ghiasvand, A. R., Noorimotlagh, Z., 2015. Removal of methylene blue and acid orange 7 from aqueous solutions by activated carbon coated with zinc oxide (ZnO) nanoparticles: equilibrium, kinetic, and thermodynamic study. Desalination Water Treat. 55, 252-262.

Rehman, M. S. U., Munir, M., Ashfaq, M., Rashid, N., Nazar, M. F., Danish, M., Han, J. I., 2013. Adsorption of Brilliant Green dye from aqueous solution onto red clay. Chem. Eng. J. 22, 54-62.

Reza, R. A., Ahmaruzzaman, M., 2015 A novel synthesis of Fe_2O_3@activated carbon composite and its exploitation for the elimination of carcinogenic textile dye from an aqueous phase. RSC Adv. 5, 10575-10586.

Roosta, M., Ghaedi, M., Daneshfar, A., Sahraei, R., Asghari, A., 2014. Optimization of the ultrasonic assisted removal of methylene blue by gold nanoparticles loaded on activated carbon using experimental design methodology. Ultrason Sonochem. 21, 242-252.

Saini, J., Garg, V. K., Gupta, R. K., 2018. Removal of Methylene Blue from aqueous solution by Fe_3O_4@Ag/SiO_2 nanospheres: Synthesis, characterization and adsorption performance. J. Mol. Liq. 250, 413–422.

Saini, J., Garg, V. K., Gupta, R. K., Kataria, N., 2017. Removal of Orange G and Rhodamine B dyes from aqueous system using hydrothermally synthesized zinc oxide loaded activated carbon (ZnO-AC). J. Environ. Chem. Eng. 5, 884–892.

Seyedsadjadi, M., Babaei, S. E., Farhadyar, N., 2014. Preparation of Surface Modified magnetic Iron Oxide nano particles and study of their colloidal behaviour. Int. J. Nano Dimens. 5, 279–289.

Smith, J.M., Ness, H.C.V., 1987. Introduction to Chemical Engineering Thermodynamics, McGraw-Hill, New York, USA.

Tan, K. A., Morad, N., Teng, T. T., Norli, I., Panneerselvam, P., 2012. Removal of cationic dye by magnetic nanoparticle (Fe_3O_4) impregnated onto activated maize cob powder and kinetic study of dye waste adsorption. APCBEE Procedia. 1, 83-89.

Temkin, M. J., Pyzhe, V., 1940. Recent modification to Langmuir Isotherms. Acta Physiochim. 12, 217-222.

Uddin, M.T., Islam, M.A., Mahmud, S., Rukanuzzaman, M., 2009. Adsorptive removal of methylene blue by tea waste. J. Hazard. Matter. 164, 53–60.

463 Wu, X. L., Shi, Y., Zhong, S., Lin, H., Chen, J. R., 2016. Facile synthesis of Fe_3O_4-
464 graphene@ mesoporous SiO_2 nanocomposites for efficient removal of Methylene Blue. Appl.
465 Surf. Sci. 378, 80-86.

466 Yazdanbakhsh, M., Tavakkoli, H., Hosseini, S. M., 2011. Characterization and evaluation
467 catalytic efficiency of $La_{0.5}Ca_{0.5}NiO$ nanopowders in removal of reactive blue 5 from aqueous
468 solution. Desalination. 281, 388–395.

469 Zargar, B., Parham, H., Rezazade, M., 2011. Fast removal and recovery of methylene blue by
470 activated carbon modified with magnetic iron oxide nanoparticles. J Chin Chem Soc. 58, 694-
471 699.

472 Zolgharnein, J., Bagtash, M., Shariatmanesh T., 2015. Simultaneous removal of binary
473 mixture of Brilliant Green and Crystal Violet using derivative spectrophotometric
474 determination, multivariate optimization and adsorption characterization of dyes on surfactant
475 modified nano-γ-alumina. Spectrochim Acta A Mol Biomol Spectrosc.137, 016-1028.

476

477

478

479

480 **Table 1: Thermodynamic parameters description of MB and BG dyes adsorption.**

Temp. (K)	Methylene Blue (MB)			Brilliant Green (BG)		
	ΔG^o (k J mol^{-1})	ΔS^o (J $mol^{-1}K^{-1}$)	ΔH^o (k J mol^{-1})	ΔG^o (k J mol^{-1})	ΔS^o (J $mol^{-1}K^{-1}$)	ΔH^o (k J mol^{-1})
283	-3.263	104.49	26.46	-2.835	92.18	22.63
298	-4.135			-5.008		
313	-5.194			-5.958		
328	-6.510			-6.660		
343	-7.912			-7.004		

481

482

483

484

485

486

487

488

489

490

491

492

493

494

495

496

497

498

499 **Table 2: Kinetic models parameters description of MB and BG dye adsorption.**

Kinetic models	Parameters	Methylene Blue (mg/L)			Brilliant Green (mg/L)		
		30	**50**	**100**	**30**	**50**	**100**
Pseudo-first	k_1 (min^{-1})	0.023	0.064	0.29	0.037	0.033	0.056
order	q_e(cal)	2.06	6.16	15.17	13.99	34.20	33.52
	R^2	0.876	0.768	0.732	0.8214	0.956	0.745
Pseudo-second	k_2 (g/mg min)	0.013	0.001	0.001	0.003	0.002	0.001
order	q_e (cal)	60.2	100.0	147.1	62.9	94.3	185.2
	R^2	0.999	0.999	0.990	0.999	0.999	0.998
Intraparticle	k_{id} (I) (mg $g^{-1}min^{-1/2}$)	0.33	3.86	2.21	5.23	4.91	14.56
diffusion	C (I)	56.2	58.9	103.6	24.1	50.4	50.3
	R^2 (I)	0.968	0.983	0.977	0.999	0.999	0.999
	k_{id} (II) (mg $g^{-1}min^{-1/2}$)	--	1.74	7.89	0.56	1.90	1.29
	C (II)	--	75.85	54.42	54.18	69.36	153.0
	R^2 (II)	--	0.897	0.947	.801	0.964	0.895
Exp. data	q_e (exp)	60.0	95.5	139.8	60.0	90.0	167.5

500

Table 3 Adsorption isotherms model parameters description of MB and BG dye adsorption.

Isotherms model	Parameters	Parameters values	
		Methylene Blue	Brilliant Green (mg/L)
Langmuir	q_{max}(mg/g)	138.8	166.6
	b(L/mg)	1.26	0.78
	R^2	0.993	0.920
Freundlich	1/n	0.222	0.248
	K_f(mg/g)	71.34	73.14
	R^2	0.923	0.916
Temkin	b_T	178.8	152.7
	K_T (L/mg)	415.4	233.4
	R^2	0.972	0.809

Table 4 Comparison of adsorption capacities of various adsorbents for MB and BG dyes

Adsorbent	Dyes	$q_{max.}$ (mg/g)	Reference
Magnetic Biochar	MB	31.25	Mubarak et al., 2015
Mt/PANI/ Fe_3O_4	MB	184.50	Mu et al., 2016
Tea waste	MB	85.16	Uddin et al., 2009
PPY/Al_2O_3composite	MB	134.77	Chen et al., 2016
Fe_3O_4-graphene@ mesoporousSiO_2	MB	139	Wu et al., 2016
Fe_3O_4@Ag/SiO_2	MB	128.4	Saini et al., 2018
AC-Magnetic Iron Oxide Nps	MB	47.62	Zargar et al., 2011
Fe3O4–charcoal	MB	97.5	Ahmed and Ahmaruzzaman, 2015
ZnO@AC nps	MB	32.2	Nourmoradi et al., 2015
Ag NPs-AC	MB	71.4	Ghaedi et al., 2012
Pd NPs-AC	MB	75.4	Ghaedi et al., 2012
Au NPs-AC	MB	185	Roosta et al., 2014
Acid Activated Carbon	MB	60.6	Arivoli et al., 2010
Fe_3O_4@AC nps	MB	138	This study
Carbon/Iron oxide nanocomposite	BG	64.1	Ahmad and Kumar, 2010
Nano-γ alumina	BG	168.593	Zolgharnein et al., 2015
Red clay	BG	125	Jia et al., 2016
ZnO nanoparticles	BG	238.1	Kataria and Garg, 2017
ZnO NP-AC	BG	142.9	Ghaedi et al., 2014
AC from Acron	BG	2.11	Ghaedi et al, 2011
Rice husk ash	BG	25.12	Mane, et al, 2007
Jute stem Activated Carbon	BG	182	Asadullah et al., 2010
Fe_3O_4@AC nps	BG	166.6	This study

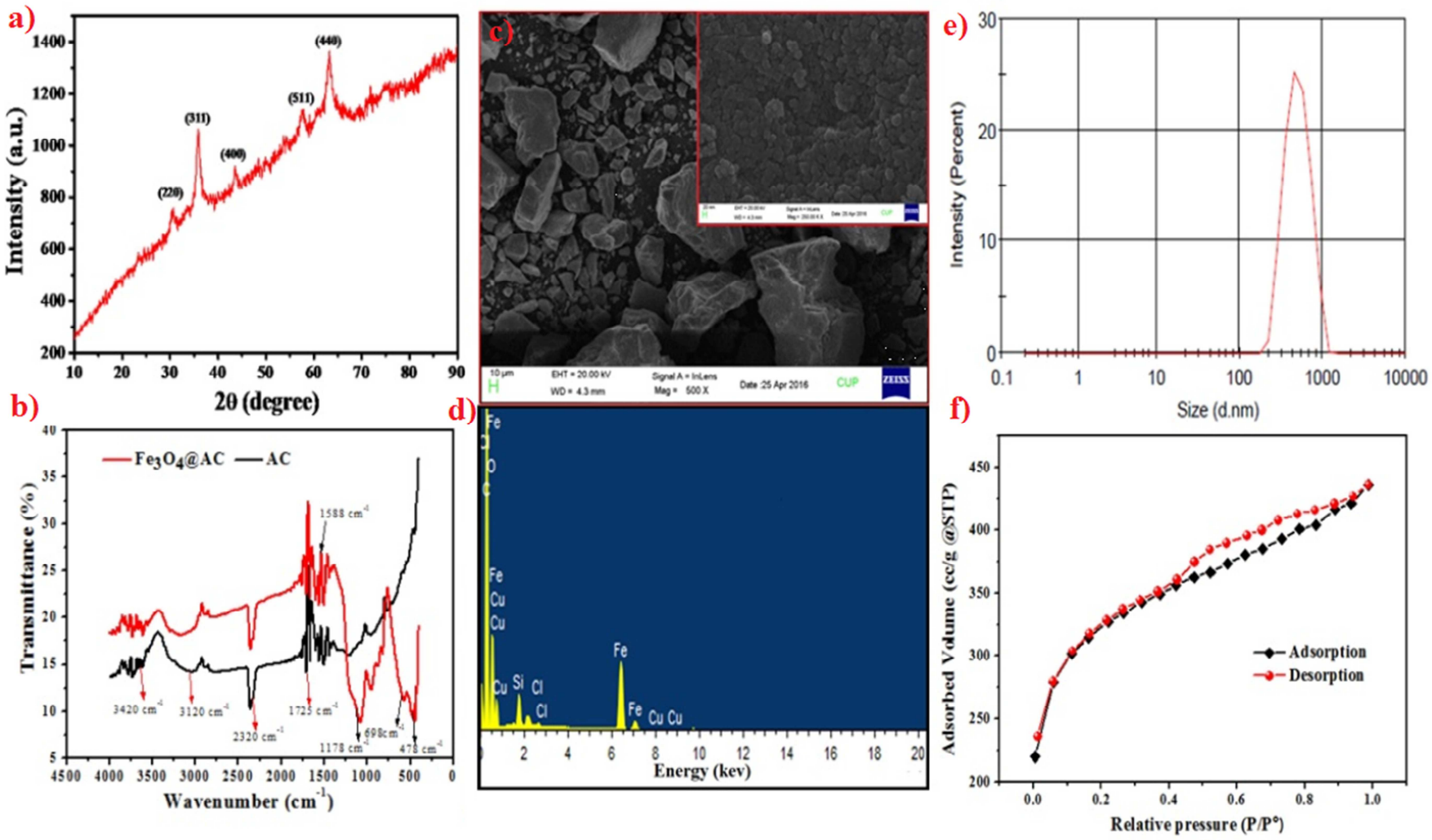

Fig. 1: a) XRD patterns of synthesized Fe_3O_4@AC nps b) FTIR spectra c) FESEM image d) EDX spectra e) DLS pattern of Fe_3O_4@AC nps and f) Nitrogen adsorption-desorption isotherms plot of Fe_3O_4@AC nps.

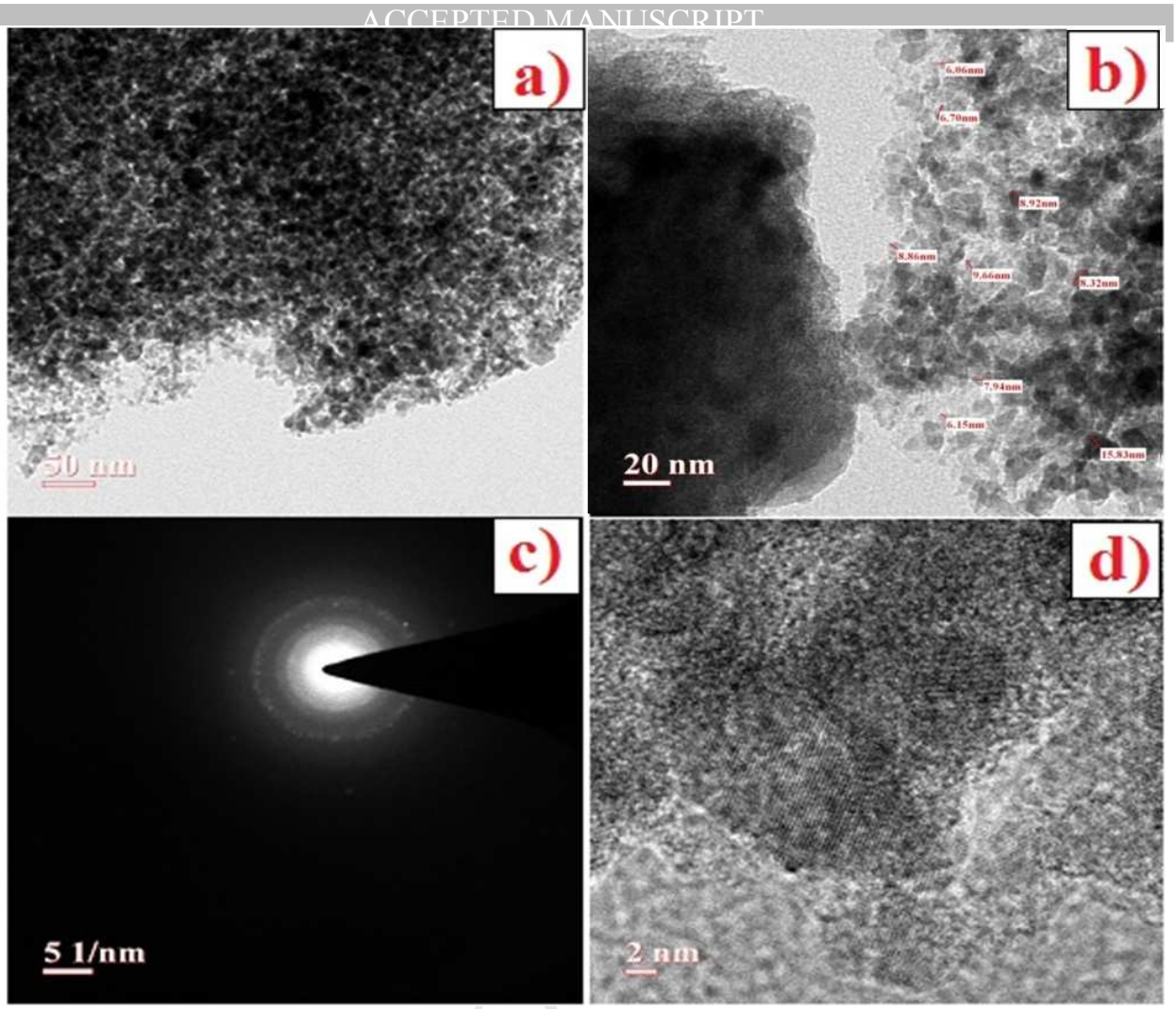

Fig 2 (a-d): TEM images of Fe_3O_4@AC nps

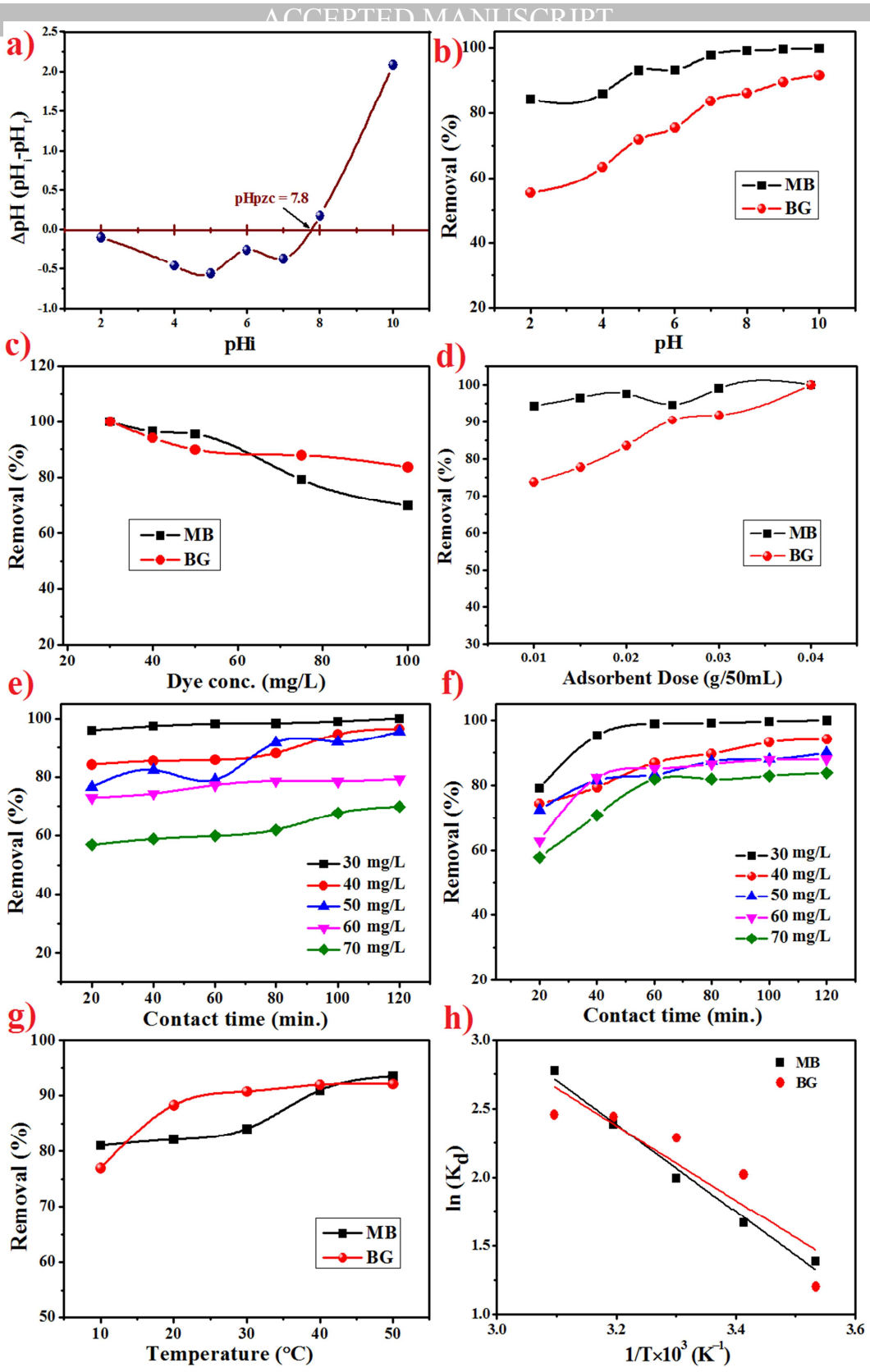

Fig. 3: a) pHpzc plots of Fe_3O_4@AC nps, b) Effect of pH, c) Effect of dye concentration, d) Effect of adsorbent dose e) Effect of contact time on adsorption of MB, f) Effect of contact time on adsorption of BG dye, g) Effect of temperature and h) Thermodynamic plot for MB and BG removal by Fe_3O_4@AC nps

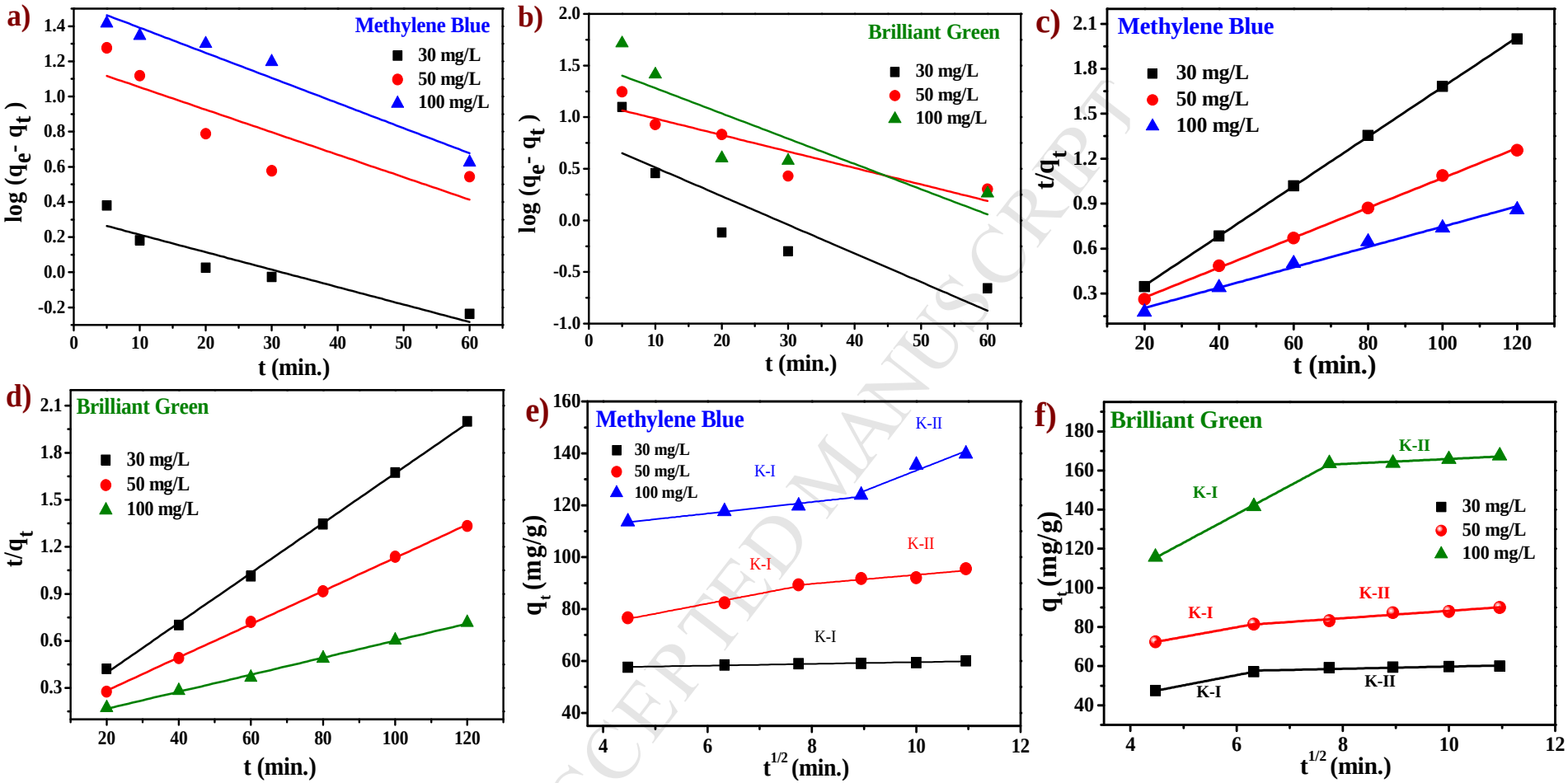

Fig 4 (a,b) Pseudo first order plot for MB and BG dye, (c,d) Pseudo second order plot for MB and BG dye and (e,f) Intraparticle diffusion models plots of MB and BG dyesadsorption on Fe_3O_4@AC nps

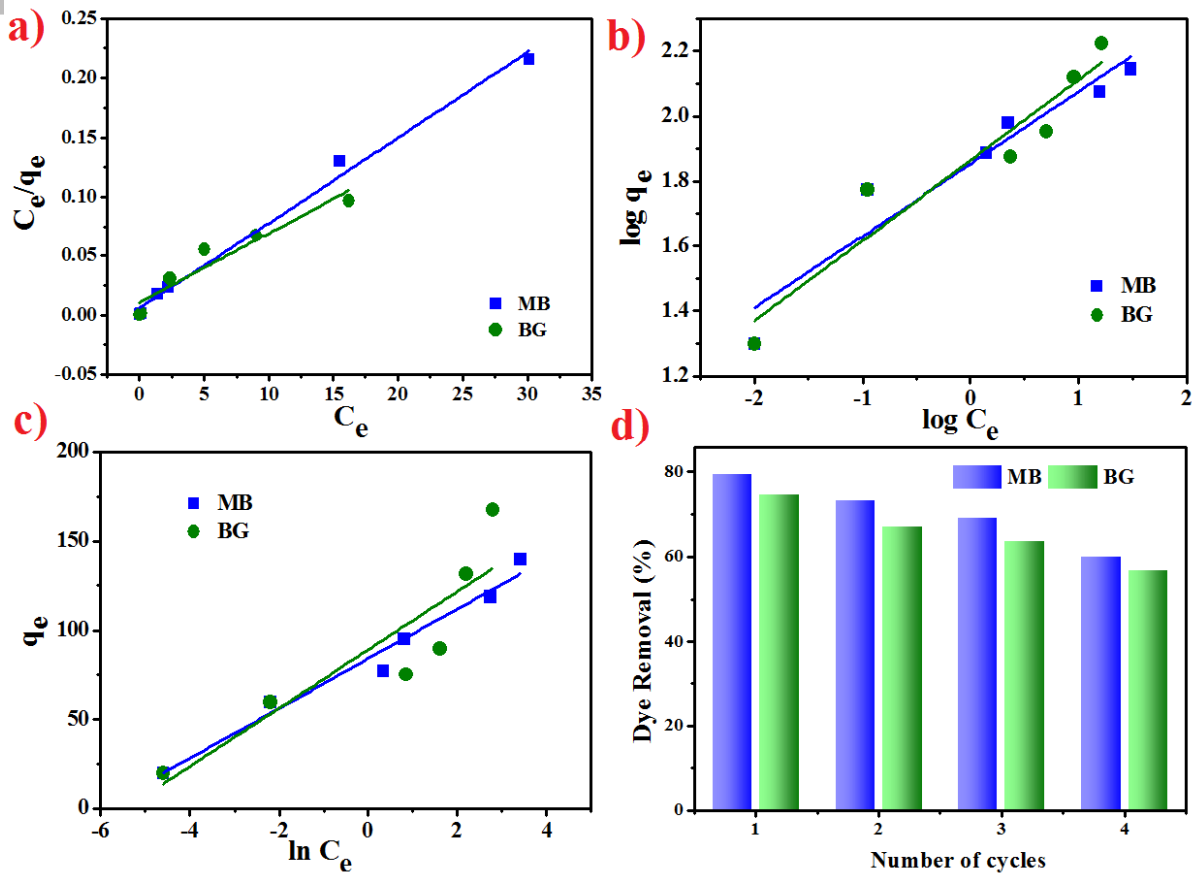

Fig 5: Adsorption isotherm plots for MB and BG dye removal by Fe_3O_4@AC nps (a) Langmuir isotherm plot (b) Freundlich isotherm plot (c) Temkin isotherm plot and d) Reuse potential of Fe_3O_4@AC nps for MB and BG dyes.

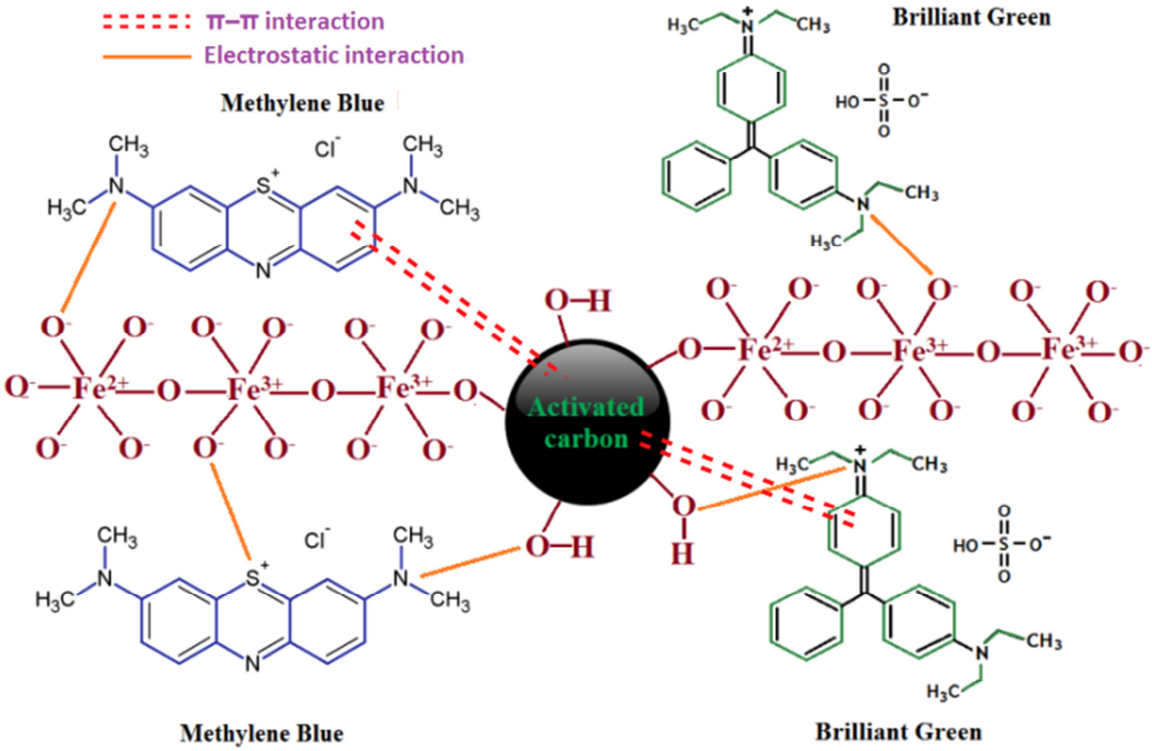

Fig 6: Possible Adsorption mechanism for dye removal onto Fe_3O_4@AC nps

Supplementary data:

Table S1 Physico-chemical properties of MB and BG dyes

Dyes	Methylene blue(MB)	Brilliant green (BG)
Molecular formula and structure	$C_{16}H_{18}N_3ClS$ 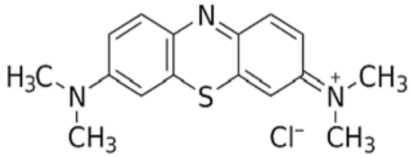	$C_{27}H_{34}N_2O_4S$ 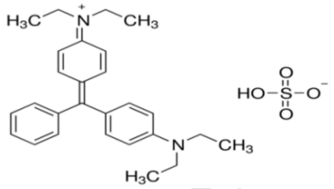
Molecular weight (g/mole)	319.85	482.63
Classification	Basic dye	Basic dye
C.I. No	52015	42040
C.I. Name	Basic blue 9	Basic green 1
Melting point (˚C)	190	210
λ_{max} (nm)	664	626

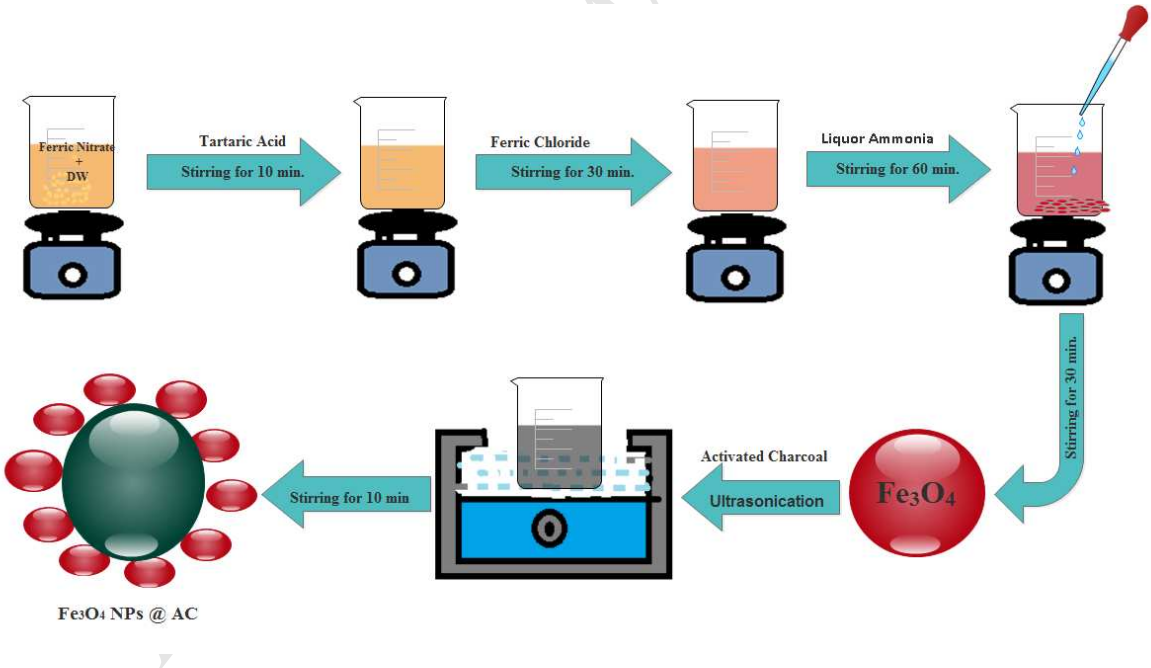

Scheme 1 Fe3O4@AC nps synthesis by co-precipitation method